HHS Public Access

Author manuscript

Mol Psychiatry. Author manuscript; available in PMC 2018 January 04.

Published in final edited form as:

Mol Psychiatry. 2018 January ; 23(1): 143–153. doi:10.1038/mp.2016.218.

Acute engagement of G_q-mediated signaling in the bed nucleus of the stria terminalis induces anxiety-like behavior

Christopher M. Mazzone, BS[1,2], **Dipanwita Pati, PhD**[2], **Michael Michaelides, PhD**[3,4,5], **Jeffrey DiBerto, BS**[2], **James H. Fox, PhD**[6], **Gregory Tipton, BS**[2], **Carlton Anderson, BS**[7], **Kelly Duffy, BS**[2], **Jessica M. McKlveen, PhD**[2], **J. Andrew Hardaway, PhD**[2], **Scott T. Magness, PhD**[9,10], **William A. Falls, PhD**[6], **Sayamwong E. Hammack, PhD**[6], **Zoe A. McElligott, PhD**[8], **Yasmin L. Hurd, PhD**[3,4], and **Thomas L. Kash, PhD**[2,11,*]

[1]Neurobiology Curriculum, University of North Carolina, Chapel Hill, NC 27599

[2]Bowles Center for Alcohol Studies, University of North Carolina School of Medicine, Chapel Hill, NC 27599

[3]Fishberg Department of Neuroscience, Friedman Brain Institute, Icahn School of Medicine at Mount Sinai, New York, NY 10029

[4]Department of Psychiatry, Friedman Brain Institute, Icahn School of Medicine at Mount Sinai, New York, NY 10029

[5]Biobehavioral Imaging and Molecular Neuropsychopharmacology Unit, Neuroimaging Research Branch, National Institute on Drug Abuse, Baltimore, MD 21224

[6]Department of Psychology, University of Vermont, Burlington, VT 05405

[7]Center for Gastrointestinal Biology and Disease, University of North Carolina, Chapel Hill, NC 27599

[8]Department of Psychiatry, University of North Carolina, Chapel Hill, NC 27599

[9]Department of Medicine, University of North Carolina, Chapel Hill, NC 27599

[10]Department of Cell Biology and Physiology, and Biomedical Engineering, University of North Carolina, Chapel Hill, NC 27599

[11]Department of Pharmacology, School of Medicine, University of North Carolina at Chapel Hill, NC, 27599

Abstract

The bed nucleus of the stria terminalis (BNST) is a brain region important for regulating anxiety-related behavior in both humans and rodents. Here we used a chemogenetic strategy to investigate how engagement of G protein-coupled receptors (GPCR) signaling cascades in genetically defined

*Address correspondence to: Thomas Kash, Laboratory of Molecular Neurophysiology, Bowles Center for Alcohol Studies, Department of Pharmacology, School of Medicine, University of North Carolina at Chapel Hill, NC, USA, tkash@email.unc.edu.

Conflict of interest

The authors declare no conflict of interest.

GABAergic BNST neurons modulates anxiety-related behavior and downstream circuit function. We saw that stimulation of vesicular γ-Aminobutyric acid (GABA) transporter (VGAT)-expressing BNST neurons using hM3Dq, but neither hM4Di nor rM3Ds Designer Receptors Exclusively Activated by a Designer Drug (DREADDs), promotes anxiety-like behavior. Further, we identified that activation of hM3Dq receptors in BNST VGAT neurons can induce a long-term depression (LTD)-like state of glutamatergic synaptic transmission, indicating DREADD-induced changes in synaptic plasticity. Further, we used DREADD-assisted metabolic mapping (DREAMM) to profile brain-wide network activity following activation of G_q-mediated signaling in BNST VGAT neurons and saw increased activity within ventral midbrain structures, including the ventral tegmental area (VTA), and hindbrain structures such as the locus coeruleus (LC) and parabrachial nucleus (PB). These results highlight that G_q-mediated signaling in BNST VGAT neurons can drive downstream network activity that correlates with anxiety-like behavior, and points to the importance of identifying endogenous GPCRs within genetically defined cell populations. We next used a microfluidics approach to profile the receptorome of single BNST VGAT neurons. This approach yielded multiple G_q-coupled receptors that are associated with anxiety-like behavior and several potential novel candidates for regulation of anxiety-like behavior. From this, we identified that stimulation of the G_q-coupled receptor 5-HT_{2C}R in the BNST is sufficient to elevate anxiety-like behavior in an acoustic startle task. Together, these results provide a novel profile of receptors within genetically defined BNST VGAT neurons that may serve as therapeutic targets for regulating anxiety states and provide a blueprint for examining how G-protein mediated signaling in a genetically defined cell type can be used to assess behavior and brain-wide circuit function.

INTRODUCTION

Anxiety disorders, including generalized anxiety disorder (GAD), panic disorder, and social anxiety disorder, are prevalent neuropsychiatric conditions. Despite decades of research and the availability of diverse pharmacological treatment options, few treatments for these disorders remain effective long-term (1–4). In order to develop better therapies, it is important to understand the complex neural networks spanning cortical, limbic, and hindbrain nuclei that control both the behavioral and autonomic components of anxiety states (5). One brain region that has long been associated with modulating such states is the bed nucleus of the stria terminalis (BNST; recently reviewed in (6,7)). This ventral forebrain structure has a large population of GABAergic neurons and has reciprocal projections with numerous limbic and hindbrain nuclei (8–10). Such diverse connectivity allows the BNST to function as a critical relay center for regulating a range of emotional and motivational processes. In humans, the BNST has elevated activity during anticipatory threat, and in rodents, broad inhibition of the BNST reduces anxiety-like behavior (11–15). However, optogenetic activation of discrete BNST outputs can also reduce anxiety-like behavior, highlighting how BNST stimulation can have opposing regulatory processes (15,16). Increased activity within the BNST is associated with elevated anxiety states in both humans (11,14,17) and non-human primates (18,19), while lesioning or pharmacological inhibition of the BNST reduces anxiety-like behavior (15,20–22). Thus, the BNST is an important nucleus in the regulation of anxiety and studies aimed at better understanding the role of the BNST in anxiety are important for the development of more effective therapeutics.

In addition to complex anatomical connectivity, the BNST expresses an array of ionotropic channels and metabotropic G-protein coupled receptors (GPCRs) for both neurotransmitter and neuropeptidergic systems (23,24). Pharmacological and *ex vivo* slice electrophysiology studies have demonstrated that local infusion of GPCR ligands into the BNST can produce changes in anxiety-like behavior and synaptic function, but the broader effects of downstream network activity remain unknown (25–30). Treatment with an α1-receptor antagonist, for example, can blunt stress-induced increases in anxiety, and restraint stress elevates norepinephrine release in the BNST (25). 5-HT_{2c} knockout (KO) mice show blunted anxiety and reduced c-fos induction in corticotropin-releasing factor (CRF)-expressing cells of the BNST following an anxiogenic stimulus (31). While these studies highlight the importance of GPCR-coupled signaling and anxiety within the BNST, they are unable to determine whether the effects are driven by pre- or postsynaptic mechanisms. Here we provide the first characterization of the behavioral and network consequences following activation of G_q-mediated signaling within BNST VGAT-expressing neurons using chemogenetic approaches. Further, we identify endogenous G_q-coupled GPCR expression in BNST VGAT neurons at the single cell level that may provide useful targets for modulating anxiety-like states.

METHODS

Mice

All animals (>8 weeks old) were group housed on a 12 hour light cycle (lights on at 7 a.m.) with *ad libitum* access to rodent chow and water, unless described otherwise. VGAT-*ires*-Cre (VGAT-Cre) mice were provided by Dr. Bradford Lowell (Harvard University) and have been described previously (32). To isolate BNST VGAT neurons for single-cell qPCR and whole-cell patch clamp electrophysiology, VGAT-Cre mice were crossed with a *Rosa26*-floxed-stop-L10-GFP reporter line (VGAT-L10)(33). Only male mice were used for behavioral, DREAMM, and single-cell profiling experiments. Male and female mice were used for electrophysiological recordings and *in situ* hybridization experiments as described below. All procedures were conducted in accordance with the National Institutes of Health guidelines for animal research and with the approval of the Institutional Animal Care and Use Committee at the University of North Carolina at Chapel Hill. For acoustic startle assessment, eight week old, male C57BL/6J mice (n = 16) were obtained from Jackson Laboratories in Bar Harbor, Maine. Mice were housed in groups of four in standard acrylic cages (24 cm (W) × 45cm (D) × 20cm (H)) located in an Association for Assessment and Accreditation of Laboratory Animal Care (AAALAC) approved conventional animal facility. Mice were maintained on a 12 h light/dark cycle (lights on at 07:00 h) with food and water available at all times. All procedures were approved by the University of Vermont Animal Care and Use Committee.

Viruses and tracers

All AAV viruses were produced by the Gene Therapy Center Vector Core at the University of North Carolina at Chapel Hill and had titers of $>10^{12}$ genome copies/mL. For chemogenetic manipulations, mice were bilaterally injected with 0.4–0.5 μl of rAAV8-hsyn-

DIO-mCherry, rAAV8-hsyn-DIO-hM3Dq-mCherry, rAAV8-hsyn-DIO-hM4Di-mCherry, or rAAV8-hsyn-DIO-rM3Ds.

Stereotaxic injections

Adult mice (>8 weeks) were deeply anesthetized with 5% isoflurane (vol/vol) in oxygen and placed into a stereotactic frame (Kopf Instruments) while on a heated pad. Sedation was maintained at 1.5–2.5% isoflurane during surgery. Following 3 alternating swabs with betadine and 70% ethanol, an incision was made down the midline of the scalp, a burr hole was drilled above the target regions, and viruses were microinjected using a 1 μl Neuros Hamilton syringe at a rate of 100 nl/min. After infusion, the needle was left in place for at least an additional 5 minutes to allow for diffusion of the virus before being slowly withdrawn. Injection coordinates for the BNST were (in mm: midline, Bregma, dorsal surface): ±0.9 − 1.10, 0.30, −4.35 (34). Following surgery, all mice were returned to group housing. Mice were allowed to recover for at least 3 weeks prior to the start of experiments.

BNST cannulation

Cannulae were obtained from Plastics One (Roanoke, VA). The cannulae used had a 22 gauge inner diameter and extended 5 mm below the 4mm pedestal. Injection cannulae had an inner diameter of 28 gauge and were 9.5 mm long and projected 0.5 mm beyond the guide cannula. Mice were anesthetized using 2% Isoflurane and oxygen and then placed into a stereotaxic instrument (Steolting, Wood Dale, Illinois). The scalps of the mice were shaved and then scrubbed in alternate with 9% betadine and 95% ethyl alcohol. The scalp was opened using a cut along the midline and then the skull was lightly scraped with the edge of a scalpel blade to remove fascia. A small burr hole was drilled in the skull where each cannula was lowered. Coordinates were 0.3 mm anterior to Bregma, 2.6 mm lateral, and 4.2 mm ventral. The cannulae were lowered at a 20 degree angle in order to avoid hitting the ventricles that lie dorsal and medial to the BNST. The same procedure was done for both the left and right BNST. After lowering both cannulae, they were affixed to the skull using glue (Loctite 454, Locktite, Westlake, OH) and a glue hardening accelerator (Loctite 7542). Mice were given 0.05mg/kg of buprenorphine prior to being removed from the sterotaxic apparatus. The mice were allowed to recover under a heat lamp prior to being returned to their home cage and the colony room. Mice were monitored daily and received 3 more doses of buprenorphine to help alleviate pain associated with the surgical procedure.

Drugs

Tetrodotoxin (TTX) and picrotoxin were purchased from Abcam, while U73122, SR 141716A, and meta-Chlorophenylpiperazine (mCPP) were purchased from Tocris. Clozapine *N*-oxide (CNO) was generously provided by Dr. Bryan Roth (University of North Carolina).

Electrophysiology

Mice were decapitated following deep isoflurane anesthesia, then brains were extracted and placed in ice-cold sucrose artificial cerebrospinal fluid (aCSF) containing (in mM) 194 sucrose, 20 NaCl, 4.4 KCl, 2 $CaCl_2$, 1 $MgCl_2$, 1.2 NaH_2PO_4, 10.0 glucose, and 26.0

$NaHCO_3$ saturated with 95% O_2/5% CO_2. Coronal sections of the BNST were sliced at 300 μm on a Leica 1200S vibratome at 0.07 mm/s. Slices were incubated in a heated holding chamber containing normal, oxygenated aCSF [(in mM): 124 NaCl, 4.4 KCl, 2 $CaCl_2$, 1.2 $MgSO_4$, 1 NaH_2PO_4, 10.0 glucose, and 26.0 $NaHCO_3$] maintained at 32 ± 1°C for at least 1 hour before recording. Slices were then transferred to a recording chamber (Warner Instruments), submerged in normal, oxygenated aCSF and maintained at 28–30°C with a flow rate of 2 ml/min and allowed to incubate for 30 minutes. Female mice were used for recordings validating Gq DREADD function and Long-term depression (LTD) experiments, while male and female mice were used to verify hM4Di-induced hyperpolarization in response to CNO. Neurons of the BNST were visualized using infrared differential interference contrast (DIC) video-enhanced microscopy (Olympus) and DREADD-expressing cells were identified by mCherry fluorescence. Whole-cell patch clamp recordings were made in current clamp mode with a potassium gluconate-based intracellular solution [(in mM): 135 K-gluconate, 5 NaCl, 2 MgCl2, 10 HEPES, 0.6 EGTA, 4 Na_2ATP, 0.4 Na_2GTP, pH 7.3, 289–292mOsmol]. To record CNO-induced depolarization of G_q-DREADD expressing VGAT neurons in the presence of 0.5 μM TTX, 10 μM CNO was bath applied for 5 minutes after a four-minute baseline. The CNO-induced depolarization was calculated as the difference between the resting membrane potential (RMP) during the last 2 minutes of CNO application and the RMP 2 minutes before CNO reached the bath. To assess the effects of phospholipase C (PLC) inhibition on CNO-induced depolarization, 10 μM U73122 was present in the bath throughout recordings. Similar recordings were obtained in G_i-DREADD expressing cells without TTX present in the bath. In G_i-DREADD-expressing cells, the rheobase, which was defined as the minimal amount of current required to elicit an action potential using a current ramp, was obtained using the potassium gluconate internal described above both before and following 5 minutes of bath application of 10 μM CNO. One cell was identified as an outlier by the Grubbs' test (alpha set to 0.01) and was excluded from the rheobase dataset. To assess the effects of G_q-DREADD activation in BNST VGAT neurons on LTD, whole cell voltage clamp recordings were obtained using a cesium-gluconate internal [(in mM): 117 Cs-gluconate, 20 HEPES, 15.2 EGTA, 83 TEA, 40 MgCl2, 200 Na_2ATP, 20 Na_2GTP, pH 7.31, 292 mOsmol] with the cell clamped at −70 mV throughout the recording period. All experiments were performed with 25 μM picrotoxin, or picrotoxin plus 5 μM SR 141716A, present in the bath. To record evoked excitatory postsynaptic currents (EPSCs), a bipolar Ni-chrome stimulated electrode was placed in the dorsal BNST and dorsal to the recorded neuron. EPSCs were evoked at a frequency of 0.167 Hz using either voltage or current pulses. Evoked experiments were analyzed in Clampfit 10.5 (Molecular Devices Sunnyvale, CA). All evoked responses were normalized to the average EPSC amplitude during the first 50 sweeps (5 mins) before CNO application. Each data point consists of a 60 second (6 sweep) average of evoked responses. In all experiments, signals were digitized at 10–20 kHz and filtered at 3 kHz using a Multiclamp 700B amplifier.

Behavioral Assays

Mice used for behavioral studies were habituated to handling for two days beginning three days prior to the first behavioral test. All behavioral testing was done during the light cycle, and there was at least 48 hours between test sessions. For chemogenetic manipulations, mice

were transported to a holding cabinet adjacent to the behavioral testing room to habituate for at least 30 minutes before being pretreated with CNO (3.0 mg/kg, i.p.) unless stated otherwise. All behavior testing began 30 minutes after CNO treatment. Equipment was cleaned with a damp cloth between mouse trials. Sessions were video recorded and analyzed using EthoVision software (Noldus Information Technologies). *Elevated Plus Maze*: Mice were placed into the center of an elevated plus maze and allowed to explore for a 5 minute session. Light levels in the open arms were ~14 lux. The probability of an open arm entry was calculated as the number of open arm entries divided by the total number of arm entries (open + closed). *Open Field*: Mice were placed into the corner of a white Plexiglas open field arena (20×20×10 cm) and allowed to freely explore for 30 minutes. The center of the open field was defined as the central 25% of the arena. Light levels were ~14 lux. *Light-Dark*: Mice were placed into the dark side of a two-compartment box containing a dark side (black walls with lid) and a light side (clear Plexiglas walls, no lid) and were allowed to freely explore for 15 minutes. The two sides were connected by a central small opening in the walls of the enclosed side. Light levels in the light side were ~300 lux in the center. *Acoustic startle*: mCPP HCl (Tocris, Ellisville, MO) was mixed fresh on the morning that behavioral testing took place. mCPP was mixed with artificial cerebral spinal fluid (aCSF) at 1 μg/.5 μl. Animals were randomly assigned to receive mCPP or vehicle with the flip of a coin. Mice received either vehicle or mCPP infusions using the injection cannula connected with polyethelene tubing to a 10ul micro syringe (Hamilton, Reno, NV). Infusions were performed with a mechanical infusion pump (KD Scientific, Holliston, MA) at a rate of 0.25ul/minute for 2 minutes for a total volume of .5ul per side. The injector cannulae were left in place for an additional 2 minutes to aid in diffusion of the drug into the target area. Behavioral testing took place immediately after infusion. The startle tests were conducted in eight sound attenuating cubicles measuring 58 cm (W) × 32 cm (D) × 55 cm (H). Each cubicle was lined with black, sound absorbing foam with no internal source of light. Each cubicle contained a stabilimeter device consisting of a load cell platform onto which the behavioral chamber was mounted (MED-ASR-PRO1, Med-Associates, Georgia, VT). The chamber was constructed from clear acrylic, cylindrical in shape, 12.5 cm in length, with an inner diameter of 5 cm. The floor of the chamber consisted of a removable grid composed of 6 steel rods 3.2 mm in diameter, and spaced 6.4 mm apart. Startle responses were transduced by the load cell, amplified, and digitized over a range of 0–4096 units. Startle amplitude was defined as the largest peak to trough value within 100 ms after the onset of the startle stimulus. After a five-minute acclimation period, mice were presented with the first of 30 startle stimulus alone trials. The startle stimulus was comprised of white noise bursts lasting for 20 milliseconds. Ten stimuli of each intensity level (95, 100, and 105 dB) were presented in a pseudo-random order (the constraint being that each intensity occur within each block of 3 trials) with an inter-trial interval (ITI) of 60 s. Data collection and the control and sequencing of all stimuli were controlled by Med-Associates startle reflex hardware and software. Raw startle scores were converted into a percent change score based on the average startle response in vehicle treated mice.

Placement Verification and Histology

All mice used for behavioral and anatomical tracing experiments were anesthetized with Avertin and transcardially perfused with 30 ml of ice-cold 0.01M PBS followed by 30 ml of

ice-cold 4% paraformaldehyde (PFA) in phosphate buffered saline (PBS). Brains were extracted and stored in 4% PFA for 24 hours at 4°C before being rinsed twice with PBS and stored in 30% sucrose/PBS until the brains sank. 45 μm slices were obtained on a Leica VT1000S and stored in 50/50 PBS/Glycerol at −20°C. DREADD-containing sections were mounted on slides, allowed to dry, coverslipped with VectaShield (Vector Labs, Burlingame, CA), and stored in the dark at 4°C. Viral injection sites were verified on either a Zeiss Axio Zoom.V16 microscope or Zeiss 800 confocal microscope. For the acoustic startle study, mice were euthanized using pentobarbital (SleepAway, Fort Dodge Drug Company, Fort Dodge, IA) and were immediately perfused transcardially using 0.9% saline followed by 10% neutral buffered formalin. Brains were saved in 10% neutral buffered formalin and coronal sections were obtained on a cryostat at 50–60um. Slices were stained with cresyl violet for cannula placement verification.

DREADD-Assisted Metabolic Mapping (DREAMM)

Male VGAT-Cre mice expressing a DIO-hM3Dq-mCherry in the BNST were fasted overnight. The next morning mice were injected with either vehicle or CNO (3 mg/kg, i.p.) and 5 minutes later were injected with [^{18}F]fluorodeoxyglucose (FDG) (~250 μCi, i.p.) and placed individually in a mouse home cage (each mouse was scanned twice). 35–40 minutes after the FDG injection mice were anesthetized with 1.5% isoflurane, placed in a prone position on the bed of an Inveon microPET scanner (Siemens Medical Solutions, Malvern, PA) and scanned using a 20 min static acquisition protocol. These time points were chosen to align with those used for behavioral testing. All scans were reconstructed using the *maximum a posteriori* (MAP) algorithm. After reconstruction, images were spatially processed and normalized using the Pixel-wise Modeling software suite (PMOD) (PMOD Inc., Zurich, Switzerland) to a mouse brain MRI template (35). Normalized scans were then analyzed using statistical parametric mapping (SPM) as previously described (36). All SPM contrasts consisted of paired t-tests within each group (e.g. VEH>CNO, VEH<CNO) and were evaluated at p=0.01. Only clusters of at least 100 contiguous voxels were reported.

FACS and Single-Cell qPCR

Single-cell suspension preparation: On two separate experimental runs, brains from one adult male VGAT-*ires*-Cre:*Rosa26*-floxed-stop-L10-GFP and one adult male mouse lacking either Cre or L10-GFP expression, were extracted following deep isoflurane anesthesia. The brains were blocked on ice to obtain a 1 mm thick coronal section containing BNST. The BNST was then isolated from the rest of the section using razor blades and was then finely minced with razor blades before being transferred to 1 ml of ice-cold Hibernate A (HA-if, Brain Bits). The samples were centrifuged for 2 minutes at 110×g at 4°C, the supernatant removed, and the pellets resuspended in 1 ml of Accutase (SCR005, Millipore) and triturated up and down 4 times before digesting the tissue for 1 hour at 4°C with end-over-end mixing. Following digestion, the tissue was centrifuged for 2 minutes at 960×g at 4°C, the supernatant was removed, and the pellets were resuspended in 0.6 ml of ice-cold Hibernate A. The samples then underwent a series of trituration steps using fire-polished glass pipettes with successively smaller diameters (1.3, 0.8, and 0.4 mm) that consisted of triturating up and down 10 times followed by placing the tube on ice for 2 minutes to allow undissociated debris to settle before collecting the supernatants and resuspending the

undissociated debris with 0.6 ml of Hibernate A. The supernatants were pooled after each trituration step. Three additional trituration steps were carried out with a 0.4 mm diameter glass pipette resulting in pooled samples of dissociated cells with a volume of ~3.6 ml. These samples were then filtered with 100 μm and 40 μm cell strainers (Falcon brand, BD Biosciences) before being used for FACS. *Single-cell isolation and qPCR*: Cells expressing VGAT-*ires*-Cre:*Rosa26*-floxed-stop-L10a-GFP were isolated by Fluorescence Activated Cell Sorting (FACS) using a Sony SH800 FACS instrument (Sony Biotechnology, San Jose, CA). Multimers were excluded using a Forward-Scatter Area (FSC-A) versus Forward-Scatter Height (FSC-H) gating strategy. Dead cells were excluded using SYTOX Blue Live/Dead stain (S34857; Thermo-Fisher Scientific, USA). Gating windows were adjusted to only include events present in the GFP+ sample relative to the GFP-control brain. ~8–9,000 VGAT-*ires*-Cre:*Rosa26*-floxed-stop-L10a-GFP cells were sorted into 20 μl of Optimem with the apoptotic inhibitor Y-27632 (Cat. #S1049, Selleck Chemical) diluted to 1:1000. Eight μl of the cell suspension (~4000 cells) was added to 2 μl of C1 resuspension buffer (Fluidigm, South San Francisco). Five μl of this cell suspension was added to a 17–25 μm Fluidigm C1 Integrated Fluidics Chip (IFC). Specific target amplification (STA) was performed on the C1 instrument according to manufacturer's specifications. The STA for each cell was interrogated for target gene (See Supplemental Table 1 for Taqman probe information) expression levels by qPCR on a 192.24 IFC using the Fluidigm Biomark HD instrument according to that standard Fluidigm protocols.

Double Fluorescence *in situ* hybridization (FISH)

For validation of the VGAT-Cre line and comparison of VGAT and GPCR cellular colocalization, mice were anesthetized using isoflurane, rapidly decapitated, and brains rapidly extracted. Female VGAT-Cre mice were used for *Slc32a1/Cre* comparisons, while male C57Bl/6 mice were used for comparisons of *Slc32a1* and GPCR expression. Immediately after removal, brains were placed on a square of aluminum foil on dry ice to freeze. Brains were then placed in a −80°C freezer for no more than 1 week before slicing. 12 μm slices containing the BNST were obtained on a Leica CM3050S cryostat (Germany) and placed directly on coverslips. FISH was performed using the Affymetrix ViewRNA 2-Plex Tissue Assay Kit with custom probes for *Slc32a1* (VGAT), *Grm5, Chrm1, Htr2c, Adra1a, Adra1b*, and *Cre* designed by Affymetrix (Santa Clara, CA). Slides were coverslipped with SouthernBiotech DAPI Fluoromount-G. (Birmingham, AL). 3×5 tiled z stack (8 optical sections comprising 10.57 μm total) were obtained on a Zeiss 800 confocal microscope. All images were preprocessed with stitching and maximum intensity projection. For quantification of *Slc32a1* and GPCR probe colocalization, 8–9 BNST images from 3 mice were hand counted using the cell counter plugin in FIJI (ImageJ). For validation of the VGAT-Cre line, 3 BNST images from 3 mice were analyzed. For all studies, cells were classified into three groups: probe 1+, probe 2+, or probe 1 and 2 +. Only cells positive for a probe were considered.

Statistics

Data are presented as means ± SEM. For comparisons with only two groups, *p* values were calculated using two-tailed paired or unpaired *t*-tests as described in the figure legends, unless specified otherwise. In cases where the data were not normally distributed, a Mann-

Whitney test was performed as listed in the figure legends. Comparisons across more than two groups were made using a one-way Analysis of Variance (ANOVA). A Tukey's posttest was performed following significance with an ANOVA. Differences were considered significant at p values below 0.05. All data were analyzed with GraphPad Prism 6 software. Figures were assembled using Adobe Illustrator.

RESULTS

Selectively targeting GABAergic neurons in the BNST

The BNST consists primarily of GABAergic neurons (8), but also contains a population of vesicular glutamate transporter 2 (vGlut2)-and vesicular glutamate transporter 3 (vGlut3)-expressing glutamatergic neurons in the ventral BNST (vBNST) (37–39). As prior reports show that stimulation of glutamatergic and GABAergic BNST outputs can evoke opposing behavioral states, we selectively targeted GABAergic BNST neurons using stereotaxic delivery of adeno-associated viruses (AAVs) encoding Cre-inducible DREADDs to the BNST of VGAT-*ires*-Cre (VGAT-Cre) mice (16) (Figure 1a). Injection of these viral constructs encoding a control mCherry fluorophore, hM3Dq-mCherry, or hM4Di-mCherry produced robust expression in both the dorsal and ventral regions of the BNST (Figure 1b). Importantly, we did not observe DREADD expression in Cre-negative littermates injected with the Cre-inducible hM3Dq (see Figure 3f). Additionally, we validated that Cre expression was limited to VGAT-expressing cells using *in situ* hybridization and observed that 99.1% of cells expressing *Cre* were positive for *Slc32a1* (VGAT) mRNA (Supplemental Figure 1). These data demonstrate that we were able to anatomically isolate BNST GABAergic cells for chemogenetic manipulations. To confirm functional DREADD expression, we recorded from hM3Dq-expressing BNST neurons using *ex vivo* whole cell slice electrophysiology (Figure 1c). Bath application of 10 μM CNO in the presence of TTX produced a 2.12 ± 0.85 mV depolarization in hM3Dq-mCherry expressing BNST VGAT neurons (Figure 1 d–e), consistent with previous reports (40–42). Bath application of the PLC inhibitor U73122 (10 μM) significantly reduced the CNO-induced depolarization (Figure 1 d–e). As PLC is a known downstream target of G_q activation, these data highlight that CNO-induced depolarization following activation of hM3Dq receptors involve canonical G_q-mediated signaling pathways. In the absence of TTX, 50% (3/6) of hM3Dq expressing neurons began firing action potentials within 5 minutes of 10 μM CNO application, while the remaining neurons showed an average depolarization of 1.69 ± 0.24 mV (data not shown). Activation of G_q-coupled receptors can also result in an LTD of postsynaptic excitatory currents (43–45). To assess if activation of hM3Dq activity within BNST VGAT neurons is sufficient to produce LTD, we recorded electrically evoked EPSCs during and following bath application of 10 μM CNO. There was a rapid and sustained reduction in EPSC amplitude relative to baseline that persisted for at least 25 minutes after washout of CNO, which was not observed in cells from non-DREADD expressing mice (Figure 1f–h). Furthermore, antagonism of the cannabinoid receptor 1 (CB_1R) with SR141716A (5 μM) blocked hM3Dq-induced LTD (Figure 1f–h). In opposition to our observations with hM3Dq activation, stimulation of the hM4Di receptor was sufficient to induce a hyperpolarization and increase the amount of current required to elicit an action

potential, thus indicating opposing actions of hM3Dq versus hM4Di signaling events (Figure 1 i–l).

Acute chemogenetic activation of BNST VGAT neurons induces anxiety-like behavior

To determine how engagement of G_q-coupled and G_i-coupled signaling in BNST VGAT neurons affects acute anxiety-like behavior, we injected Cre-inducible hM3Dq or hM4Di constructs into the BNST of VGAT-*ires*-Cre mice with a Cre-inducible mCherry used as a control. Mice were treated with CNO (3.0 mg/kg) 30 minutes before testing to allow time for DREADD-induced changes in activity (Figure 2a). In the elevated plus maze (EPM, Figure 2b), DREADD activation did not alter locomotor activity, but hM3Dq-expressing mice spent less time in the open arms and had a significantly reduced likelihood of entering an open arm. In the open field, neither the hM3Dq-expressing nor the hM4Di-expressing group showed changes in distance traveled (Figure 2e, left), time spent in the center of the open field, or latency to enter the center of the open field (Figure 2e, center and right, respectively). In the light-dark test, only the hM3Dq-expressing mice spent less time in the light compartment and made fewer entrances to the light side (Figure 2f). Separately, we observed that acute activation of G_s-coupled signaling using the rM3Ds DREADD construct did not change anxiety in the same assays relative to mCherry controls (Supplemental Figure 2). These results indicate that acute engagement of G_q-coupled, but neither G_i-nor G_s-coupled, signaling in BNST VGAT neurons is sufficient to generate an anxiety-like state in specific contexts.

Metabolic mapping of BNST VGAT hM3Dq-evoked activity reveals broad circuit engagement

The BNST sends projections to many structures involved with reward, anxiety, and the regulation of autonomic function (9,15). Injection of a Cre-inducible mCherry to the BNST of a VGAT-Cre mouse (Figure 3a) showed direct projections of BNST VGAT fibers to these established regions, including the ventral tegmental area (VTA), locus coeruleus (LC), or parabrachial nucleus (PBN) (Figure 3b). Given that we observed increases in anxiety-like behavior following the activation of G_q-coupled DREADDs in BNST VGAT neurons, we hypothesized that engagement of G_q-mediated signaling within BNST VGAT neurons could produce extensive changes in network dynamics in these downstream targets. We used DREADD-assisted metabolic mapping (DREAMM) (46,47) to assess how activation of hM3Dq receptors in BNST VGAT neurons alters network activity. VGAT-Cre mice expressing DIO-hM3Dq in the BNST underwent two imaging sessions following both vehicle and CNO pre-treatment. Five minutes after this pre-treatment, mice were injected with [^{18}F]fluorodeoxyglucose (FDG) before being anesthetized with isoflurane 25 minutes later and undergoing scanning (Figure 3c). Mice with hM3Dq expression in the BNST (Figure 3d) showed increases in FDG uptake in the BNST, ventral tegmental area (VTA), the locus coeruleus (LC), and the parabrachial nucleus (PBN) (Figure 3e). Interestingly, we also observed elevated FDG uptake in the medial prefrontal cortex (mPFC), somatosensory cortex, and the central nucleus of the amygdala (CeA) (see Supplemental Video 1). Cre-negative littermates injected with a DIO-hM3Dq-mCherry lacked DREADD expression and showed neglibile CNO-induced changes in FDG uptake in these regions (Figure 3f–g, Supplemental Video 2).

Single-cell profiling of BNST VGAT cells highlights endogenous transcription of G_q-coupled GPCRs

As we observed robust changes in anxiety-like behavior following activation of G_q signaling in hM3Dq-expressing, but neither hM4Di- nor rM3Ds-expressing BNST VGAT neurons, we sought a greater understanding of the range of endogenous G_q-coupled receptors expressed within these cells. To isolate this population, the BNST was dissected from VGAT-Cre mice crossed with a flox-stop L10-EGFP reporter line. After creating a single-cell suspension, we isolated EGFP positive cells using fluorescence-activated cell sorting (FACS), then captured sorted cells using a Fluidigm C1 microfluidics chip. Captured cells were lysed and used for single-cell quantitative polymerase chain reaction (qPCR) with probes targeting Slc32a1 (VGAT), Map2 (a neuronal marker), Gad1 and Gad2 (GABA markers), and an array of G_q-coupled receptors (Figure 4a–b). We were able to capture 163 cells from two samples collected from two individual mice run on two separate chips. Our *a priori* exclusion criteria removed from analysis any cells negative for VGAT (13/163), Map2 (0/163), or both Gad1 and Gad2 (1/163), resulting in 149 remaining cells. Interestingly, none of the excluded cells were positive for *Slc17a6* (vGlut2), and only 1 cell was positive for *Slc17a8* (vGlut3). Of the remaining 149 cells, we observed that greater than 50% of captured cells expressed transcripts for the G_q-coupled receptors *Grm5* (93.3%), *Ntsr2* (85.2%), *Chrm1* (71.1%), *Htr2c* (55.7%), or *Grm1* (50.3%) (Figure 4c). We next used fluorescence *in situ* hybridization (FISH) to validate our qPCR findings by examining colocalization of mRNA for VGAT and various GPCRs (Figure 4d–i). In agreement with the microfluidics approach, we observed a similar distribution of the probed GPCRs in VGAT mRNA positive cells (Figure 4i). Together, these results reveal an array of endogenous G_q-coupled receptors expressed within a genetically defined cell population in the BNST.

Infusion of a 5-HT_{2C}R agonist in the BNST increases anxiety-like behavior

Of the identified endogenous G_q-coupled receptors identified in BNST VGAT neurons, we selected the 5-HT_{2C}R for further analysis. The 5-HT system is known to be involved in anxiety and other affective-related behaviors, including within the BNST (48–50). We implanted cannulae over the BNST and locally infused the 5-HT_{2C}R agonist mCPP immediately before testing in an acoustic startle task. Briefly, mice were placed on an accelerometer in a sound-attenuated chamber then presented with short noise burst. The magnitude of the startle served as an index of anxiety-like behavior. Bilateral infusion of mCPP (1 μg) into the BNST reliably increased acoustic startle responding relative to vehicle treated controls, thus indicating that activation of this G_q-coupled receptor leads to an increase in anxiety-like behavior (Figure 5).

DISCUSSION

Existing pharmacological options for anxiety disorders remain ineffective in many patients and are often accompanied by undesirable side effects (1,4). Therapeutic difficulties arise, in part, due to the incomplete understanding of cell populations and brain circuits involved in mediating the desirable effects of drug treatments. Advances in optogenetic and chemogenetic techniques have revealed how stimulation of specific cell types within a structure can drive pathological behavior. However, many of these studies to date have

focused on well-known anatomical pathways, and few have capitalized on discovery-based tools to identify novel endogenous modulators of function. Here we use a chemogenetic strategy to probe the role of GPCR signaling within a genetically defined cell population involved in anxiety-like behavior. We show that engagement of G_q-mediated signaling in BNST VGAT-expressing neurons induces anxiety-like behavior, while acute activation of both G_i and G_s signaling is insufficient to change anxiety-like responses in the assays tested. DREAMM imaging analysis following activation of G_q-DREADD signaling in BNST VGAT neurons showed enhanced activity in brain areas including the VTA, LC, and PBN. Furthermore, we used a discovery-based approach to identify potential novel GPCR regulators of this cell population. These results not only provide an anatomical framework for anxiety-like behavior, but a conceptual framework to parse out novel GPCR regulators of circuit function and behavior.

While hM3Dq-treated mice showed increased anxiety-like behavior, it is interesting that we did not see reductions in anxiety-like behavior following activation of hM4Di signaling, particularly in light of previous work showing that pharmacological or optical inhibition of the BNST reduces anxiety behavior (15). At rest, the BNST has low levels of activity, and it is possible that the environment for our assays was not sufficient to engage BNST function. As the hM4Di DREADD produced a hyperpolarizing inhibitory effect (Figure 1), suppressing activity of the BNST in these contexts may be insufficient to further reduce anxiety-like behavior. It would be interesting to repeat these experiments with activation of hM4Di DREADDs during a stressor that is known to increase BNST activity (foot shock, restraint, etc.) immediately before anxiety testing. Alternatively, similar experiments could be performed under brighter lighting conditions, as previous work has shown that open field exposure under bright lights (~600 lux) increases c-fos expression in the BNST (31). Likewise, we did not see changes in anxiety-like behavior following manipulation of G_s-coupled signaling. While G_q- and G_s-coupled receptors have stimulatory effects, a recent study identified that activation of G_q- and G_s-coupled DREADDs in agouti-related peptide (AgRP) neurons of the hypothalamus promoted feeding behavior through independent mechanisms, and that only G_s DREADD activation promoted AgRP release (51). As the BNST expresses an array of peptides, including corticotropin-releasing factor (CRF) and neuropeptide Y (NPY) that are known to produce opposing behavioral responses, it is possible that potential stimulation of peptide release in BNST VGAT neurons using the G_s-coupled DREADD occludes the effect of activation of these individual peptide receptors alone (52–56).

In addition to observing G_q-induced changes in behavior, our *ex vivo* slice electrophysiology recordings identified that activation of hM3Dq receptors in BNST VGAT neurons produced stimulatory depolarizing effects capable of increasing action potential firing that were accompanied by an LTD-like reduction of evoked EPSCs that persisted at least 25 minutes following washout of CNO. These changes are in agreement with previous studies demonstrating that bath application of agonists for the G_q-coupled α_1-adrenergic receptor or group I metabotropic glutamate receptors induces LTD in the BNST (43–45). Similarly, in the CA1 region of the hippocampus, stimulation of G_q-coupled DREADDs alters long-term plasticity, including LTD and long-term potentiation (LTP) as assessed by field recordings (57). It is important to note, however, that while G_q-induced LTD has been observed in the

BNST, we are currently unable to selectively antagonize the hM3Dq receptor following LTD induction to confirm the observed changes in synaptic plasticity are independent of CNO remaining bound to the DREADD receptor. Interestingly, we observed that the hM3Dq-induced reductions in EPSC amplitude involved CB_1R-dependent activity, in agreement with previous long-term plasticity reports indicating CB_1R-dependent reductions in evoked EPSC amplitude in the BNST (43,58).

Our results from DREAMM analysis point to changes in metabolic activity throughout brain regions previously associated with anxiety pathology, including the mPFC, CeA, VTA, PBN, and the somatosensory cortex (5,59–62). Of note, we observed no reductions in regional metabolic activity following CNO treatment. Other studies assessing brain glucose metabolism during periods of anxiety have also observed enhanced metabolic activity in subcortical and limbic regions across species including rats, monkeys, and humans (18,63–65). Importantly, FDG uptake represents increased glucose uptake and would therefore also be observed in active presynaptic terminals (46). Therefore, the exclusive increase in activity may reflect both enhanced presynaptic activity of BNST GABAergic afferents and increased local activity resulting from polysynaptic disinhibition. In agreement with this, previous work has shown that GABAergic BNST projections to the VTA innervate GABAergic VTA neurons (16). However, the BNST to VTA projection is unlikely to account for the anxiogenic phenotype reported here as that study demonstrated that optogenetic stimulation results in anxiolysis. Nonetheless, given that stimulation of G_q-mediated signaling in BNST VGAT neurons was sufficient to induce anxiety, the observed changes in metabolic activity throughout the brain may highlight a potential biomarker for pathological anxiety.

While the results reported here reflect acute activation of BNST VGAT neurons and corresponding increases in anxiety, changes in BNST neuronal activity have been observed under other models of pathological anxiety. For example, we recently found that BNST neurons exhibited increased excitability following chronic alcohol exposure, and that elevated BNST excitability correlated with increased anxiety-like behavior (66). Moreover, we previously found that the increase in excitability was associated with excessive $5\text{-}HT_{2C}R$ mediated signaling (67), and here we identify that an agonist of $5\text{-}HT_{2C}R$ in the BNST increases anxiety-like startle responding. The approach outlined in this study provides a framework for identifying GPCRs that may be differentially altered during anxiety states. Additionally, the application of whole brain imaging using these genetic approaches provides a robust and reproducible approach for connecting cellular signaling events to broad patterns of activity. Identification of brain-wide network activity patterns is especially important as this provides a point of translation for human studies. For example, the new Research Domain Criteria (RDoC) system proposed by the National Institute of Mental Health as a means for understanding brain disorders, suggests that identifying the circuit elements associated with specific endophenotypes across multiple disorders can provide insight into treatment. One such RDoC construct is potential threat or anxiety. Our work highlights a whole brain metabolic map that could potentially serve as a biomarker for heterogeneous populations of patients suffering from conditions co-morbid with anxiety disorders and identifies potential receptor targets that may drive this endophenotype. Our results presented here in the naive state lay the foundation for future work to assess how the development of pathological anxiety states, such as anxiety associated with withdrawal from

chronic alcohol exposure, changes GPCR expression patterns in BNST VGAT neuron and correspondingly changes metabolic brain-wide activity patterns.

Supplementary Material

Refer to Web version on PubMed Central for supplementary material.

Acknowledgments

We would like to thank Dr. Francisco Javier Rubio Gallego for providing the protocol used for single-cell dissociations. FACS and Fluidigm experiments were conducted by the UNC Advanced Analytics Core (Center for GI Biology and Disease; P30 DK034987). This work was supported by the National Institute on Drug Abuse (NIDA; DA015446, DA033660, DA030359). M.M. was supported by the NIDA Postdoctoral Training Program at Icahn School of Medicine at Mount Sinai (DA007135). J.A.H was funded by MH076694. C.M.M. was funded by F31 AA023440 from the National Institute on Alcohol Abuse and Alcoholism. T.L.K. was funded by P60 AA011605, R01 AA019454, U01 AA020911, and U01 MH105892. J.M.M. is supported by an Institutional Postdoctoral NRSA T32 AA007573. Z.A.M. was funded by K01 AA023555 and the Alcohol Beverage Medical Research Fund. The acoustic startle experiment was funded by MH080935 (S.E.H.). M.M. owns stock in Metis Laboratories, Inc.

REFERENCES

1. Griebel G, Holmes A. 50 years of hurdles and hope in anxiolytic drug discovery. Nat Rev Drug Discov. Nature Publishing Group. 2013 Aug 30; 12(9):667–687.
2. Kessler RC, Chiu WT, Demler O, Walters EE. Prevalence, Severity, and Comorbidity of 12-Month DSM-IV Disorders in the National Comorbidity Survey Replication. Arch Gen Psychiatry. 2005 Jun 1.62(6):617. [PubMed: 15939839]
3. Kessler RC, Berglund P, Demler O, Jin R, Merikangas KR, Walters EE. Lifetime Prevalence and Age-of-Onset Distributions of DSM-IV Disorders in the National Comorbidity Survey Replication. Arch Gen Psychiatry. 2005 Jun 1.62(6):593. [PubMed: 15939837]
4. Insel TR. Next-generation treatments for mental disorders. Sci Transl Med. 2012 Oct 10.4(155): 155ps19.
5. Calhoon GG, Tye KM. Resolving the neural circuits of anxiety. Nat Neurosci. 2015 Oct 25; 18(10): 1394–1404. [PubMed: 26404714]
6. Daniel SE, Rainnie DG. Stress Modulation of Opposing Circuits in the Bed Nucleus of the Stria Terminalis. Neuropsychopharmacology. Nature Publishing Group. 2016 Jan 22; 41(1):103–125.
7. Lebow MA, Chen A. Overshadowed by the amygdala: the bed nucleus of the stria terminalis emerges as key to psychiatric disorders. Mol Psychiatry. Nature Publishing Group. 2016 Apr; 21(4): 450–463.
8. Sun N, Cassell MD. Intrinsic GABAergic neurons in the rat central extended amygdala. J Comp Neurol. 1993 Apr 15; 330(3):381–404. [PubMed: 8385679]
9. Dong H-W, Swanson LW. Organization of axonal projections from the anterolateral area of the bed nuclei of the stria terminalis. J Comp Neurol. 2004 Jan 6; 468(2):277–298. [PubMed: 14648685]
10. Dong H-W, Swanson LW. Projections from bed nuclei of the stria terminalis, anteromedial area: cerebral hemisphere integration of neuroendocrine, autonomic, and behavioral aspects of energy balance. J Comp Neurol. 2006 Jan 1; 494(1):142–178. [PubMed: 16304685]
11. Straube T, Mentzel H-J, Miltner WHR. Waiting for spiders: brain activation during anticipatory anxiety in spider phobics. Neuroimage. 2007 Oct 1; 37(4):1427–1436. [PubMed: 17681799]
12. Mobbs D, Yu R, Rowe JB, Eich H, FeldmanHall O, Dalgleish T. Neural activity associated with monitoring the oscillating threat value of a tarantula. Proc Natl Acad Sci. 2010 Nov 23; 107(47): 20582–20586. [PubMed: 21059963]
13. Mobbs D, Petrovic P, Marchant JL, Hassabis D, Weiskopf N, Seymour B, et al. When fear is near: threat imminence elicits prefrontal-periaqueductal gray shifts in humans. Science. 2007; 317(5841):1079–1083. [PubMed: 17717184]

14. Somerville LH, Whalen PJ, Kelley WM. Human bed nucleus of the stria terminalis indexes hypervigilant threat monitoring. Biol Psychiatry. Elsevier Inc. 2010 Sep 1; 68(5):416–424.
15. Kim S-Y, Adhikari A, Lee SY, Marshel JH, Kim CK, Mallory CS, et al. Diverging neural pathways assemble a behavioural state from separable features in anxiety. Nature. Nature Publishing Group. 2013 Mar 20; 496(7444):219–223.
16. Jennings JH, Sparta DR, Stamatakis AM, Ung RL, Pleil KE, Kash TL, et al. Distinct extended amygdala circuits for divergent motivational states. Nature. Nature Publishing Group. 2013 Mar 20.
17. Yassa MA, Hazlett RL, Stark CEL, Hoehn-Saric R. Functional MRI of the amygdala and bed nucleus of the stria terminalis during conditions of uncertainty in generalized anxiety disorder. J Psychiatr Res. Elsevier Ltd. 2012; 46(8):1045–1052.
18. Fox AS, Shelton SE, Oakes TR, Davidson RJ, Kalin NH. Trait-like brain activity during adolescence predicts anxious temperament in primates. PLoS One. 2008; 3(7):e2570. [PubMed: 18596957]
19. Kalin NH, Shelton SE, Fox AS, Oakes TR, Davidson RJ. Brain Regions Associated with the Expression and Contextual Regulation of Anxiety in Primates. Biol Psychiatry. 2005; 58(10):796–804. [PubMed: 16043132]
20. Lee Y, Davis M. Role of the hippocampus, the bed nucleus of the stria terminalis, and the amygdala in the excitatory effect of corticotropin-releasing hormone on the acoustic startle reflex. J Neurosci. 1997 Aug 15; 17(16):6434–6446. [PubMed: 9236251]
21. Walker DL, Davis M. Double dissociation between the involvement of the bed nucleus of the stria terminalis and the central nucleus of the amygdala in startle increases produced by conditioned versus unconditioned fear. J Neurosci. 1997; 17(23):9375–9383. [PubMed: 9364083]
22. Waddell J, Morris RW, Bouton ME. Effects of bed nucleus of the stria terminalis lesions on conditioned anxiety: Aversive conditioning with long-duration conditional stimuli and reinstatement of extinguished fear. Behav Neurosci. 2006; 120(2):324–336. [PubMed: 16719697]
23. Kash TL. The role of biogenic amine signaling in the bed nucleus of the stria terminals in alcohol abuse. Alcohol. Elsevier Ltd. 2012 Jun 24; 46(4):303–308.
24. Kash TL, Pleil KE, Marcinkiewcz CA, Lowery-Gionta EG, Crowley N, Mazzone C, et al. Neuropeptide Regulation of Signaling and Behavior in the BNST. Mol Cells. 2015 Jan 31; 38(1): 1–13. [PubMed: 25475545]
25. Cecchi M, Khoshbouei H, Javors M, Morilak Da. Modulatory effects of norepinephrine in the lateral bed nucleus of the stria terminalis on behavioral and neuroendocrine responses to acute stress. Neuroscience. 2002 Jan; 112(1):13–21. [PubMed: 12044468]
26. Walker DL, Miles LA, Davis M. Selective participation of the bed nucleus of the stria terminalis and CRF in sustained anxiety-like versus phasic fear-like responses. Prog Neuro-Psychopharmacology Biol Psychiatry. Elsevier Inc. 2009 Nov 13; 33(8):1291–1308.
27. Walker D, Yang Y, Ratti E, Corsi M, Trist D, Davis M. Differential Effects of the CRF-R1 Antagonist GSK876008 on Fear-Potentiated, Light- and CRF-Enhanced Startle Suggest Preferential Involvement in Sustained vs Phasic Threat Responses. Neuropsychopharmacology. Nature Publishing Group. 2009 May; 34(6):1533–1542.
28. Hammack SE, Cheung J, Rhodes KM, Schutz KC, Falls Wa, Braas KM, et al. Chronic stress increases pituitary adenylate cyclase-activating peptide (PACAP) and brain-derived neurotrophic factor (BDNF) mRNA expression in the bed nucleus of the stria terminalis (BNST): Roles for PACAP in anxiety-like behavior. Psychoneuroendocrinology. 2009 Jul; 34(6):833–843. [PubMed: 19181454]
29. Levita L, Hammack SE, Mania I, Li X-Y, Davis M, Rainnie DG. 5-hydroxytryptamine1a-likereceptor activation in the bed nucleus of the stria terminalis: Electrophysiological and behavioral studies. Neuroscience. 2004 Jan; 128(3):583–596. [PubMed: 15381287]
30. Fox JH, Hammack SE, Falls Wa. Exercise is associated with reduction in the anxiogenic effect of mCPP on acoustic startle. Behav Neurosci. 2008 Aug; 122(4):943–948. [PubMed: 18729648]
31. Heisler LK, Zhou L, Bajwa P, Hsu J, Tecott LH. Serotonin 5-HT(2C) receptors regulate anxiety-like behavior. Genes Brain Behav. 2007 Jul; 6(5):491–496. [PubMed: 17451451]

32. Vong L, Ye C, Yang Z, Choi B, Chua S, Lowell BB. Leptin Action on GABAergic Neurons Prevents Obesity and Reduces Inhibitory Tone to POMC Neurons. Neuron. 2011 Jul; 71(1):142–154. [PubMed: 21745644]
33. Krashes MJ, Shah BP, Madara JC, Olson DP, Strochlic DE, Garfield AS, et al. An excitatory paraventricular nucleus to AgRP neuron circuit that drives hunger. Nature. Nature Publishing Group. 2014 Feb 2.
34. Franklin, KBJ., Paxinos, G. The Mouse Brain in Stereotaxic Coordinates, Compact Third Edition. New York, NY: Elsevier; 2008.
35. Michaelides M, Pascau J, Gispert JD, Delis F, Grandy DK, Wang GJ, et al. Dopamine D4 receptors modulate brain metabolic activity in the prefrontal cortex and cerebellum at rest and in response to methylphenidate. Eur J Neurosci. 2010; 32(4):668–676. [PubMed: 20646063]
36. Urban DJ, Zhu H, Marcinkiewcz CA, Michaelides M, Oshibuchi H, Rhea D, et al. Elucidation of the Behavioral Program and Neuronal Network Encoded by Dorsal Raphe Serotonergic Neurons. Neuropsychopharmacology. Nature Publishing Group. 2015:1–12.
37. Hur EE, Zaborszky L. Vglut2 afferents to the medial prefrontal and primary somatosensory cortices: A combined retrograde tracing in situ hybridization. J Comp Neurol. 2005 Mar 14; 483(3):351–373. [PubMed: 15682395]
38. Poulin J-F, Arbour D, Laforest S, Drolet G. Neuroanatomical characterization of endogenous opioids in the bed nucleus of the stria terminalis. Prog Neuro-Psychopharmacology Biol Psychiatry. 2009 Nov 13; 33(8):1356–1365.
39. Kudo T, Uchigashima M, Miyazaki T, Konno K, Yamasaki M, Yanagawa Y, et al. Three Types of Neurochemical Projection from the Bed Nucleus of the Stria Terminalis to the Ventral Tegmental Area in Adult Mice. J Neurosci. 2012 Dec 12; 32(50):18035–18046. [PubMed: 23238719]
40. Krashes MJ, Koda S, Ye C, Rogan SC, Adams AC, Cusher DS, et al. Rapid, reversible activation of AgRP neurons drives feeding behavior in mice. J Clin Invest. 2011 Apr 1; 121(4):1424–1428. [PubMed: 21364278]
41. Alexander GM, Rogan SC, Abbas AI, Armbruster BN, Pei Y, Allen Ja, et al. Remote control of neuronal activity in transgenic mice expressing evolved G protein-coupled receptors. Neuron. Elsevier Ltd. 2009 Jul 16; 63(1):27–39.
42. Yiu AP, Mercaldo V, Yan C, Richards B, Rashid AJ, Hsiang H-LL, et al. Neurons Are Recruited to a Memory Trace Based on Relative Neuronal Excitability Immediately before Training. Neuron. Elsevier Inc. 2014 Aug; 83(3):722–735.
43. Grueter BA, Gosnell HB, Olsen CM, Schramm-Sapyta NL, Nekrasova T, Landreth GE, et al. Extracellular-signal regulated kinase 1-dependent metabotropic glutamate receptor 5-induced long-term depression in the bed nucleus of the stria terminalis is disrupted by cocaine administration. J Neurosci. 2006 Mar 22; 26(12):3210–3219. [PubMed: 16554472]
44. McElligott, Za, Klug, JR., Nobis, WP., Patel, S., Grueter, BA., Kash, TL., et al. Distinct forms of Gq-receptor-dependent plasticity of excitatory transmission in the BNST are differentially affected by stress. Proc Natl Acad Sci. 2010 Feb 2; 107(5):2271–2276. [PubMed: 20133871]
45. McElligott ZA, Winder DG. Alpha1-adrenergic receptor-induced heterosynaptic long-term depression in the bed nucleus of the stria terminalis is disrupted in mouse models of affective disorders. Neuropsychopharmacology. 2008 Sep 28; 33(10):2313–2323. [PubMed: 18046308]
46. Michaelides M, Anderson SAR, Ananth M, Smirnov D, Thanos PK, Neumaier JF, et al. Whole-brain circuit dissection in free-moving animals reveals cell-specific mesocorticolimbic networks. J Clin Invest. 2013 Dec 2; 123(12):5342–5350. [PubMed: 24231358]
47. Anderson SAR, Michaelides M, Zarnegar P, Ren Y, Fagergren P, Thanos PK, et al. Impaired periamygdaloid-cortex prodynorphin is characteristic of opiate addiction and depression. J Clin Invest. 2013 Dec 2; 123(12):5334–5341. [PubMed: 24231353]
48. Burghardt NS, Sullivan GM, McEwen BS, Gorman JM, LeDoux JE. The selective serotonin reuptake inhibitor citalopram increases fear after acute treatment but reduces fear with chronic treatment: a comparison with tianeptine. Biol Psychiatry. 2004 Jun 15; 55(12):1171–1178. [PubMed: 15184036]

49. Ravinder S, Burghardt NS, Brodsky R, Bauer EP, Chattarji S. A role for the extended amygdala in the fear-enhancing effects of acute selective serotonin reuptake inhibitor treatment. Transl Psychiatry. Nature Publishing Group. 2013 Jan.3(1):e209.
50. Marcinkiewcz CA, Mazzone CM, D'Agostino G, Halladay LR, Hardaway JA, DiBerto JF, et al. Serotonin engages an anxiety and fear-promoting circuit in the extended amygdala. Nature. Nature Publishing Group. 2016 Aug 24.:1–19.
51. Nakajima K, Cui Z, Li C, Meister J, Cui Y, Fu O, et al. Gs-coupled GPCR signalling in AgRP neurons triggers sustained increase in food intake. Nat Commun. 2016 Jan 8.7:10268. [PubMed: 26743492]
52. Pleil KE, Rinker JA, Lowery-Gionta EG, Mazzone CM, McCall NM, Kendra AM, et al. NPY signaling inhibits extended amygdala CRF neurons to suppress binge alcohol drinking. Nat Neurosci. 2015; 18(November 2014):545–552. [PubMed: 25751534]
53. Kash TL, Winder DG. Neuropeptide Y and corticotropin-releasing factor bi-directionally modulate inhibitory synaptic transmission in the bed nucleus of the stria terminalis. Neuropharmacology. 2006 Oct; 51(5):1013–1022. [PubMed: 16904135]
54. Valdez GR, Koob GF. Allostasis and dysregulation of corticotropin-releasing factor and neuropeptide Y systems: implications for the development of alcoholism. Pharmacol Biochem Behav. 2004 Dec; 79(4):671–689. [PubMed: 15582675]
55. Heilig M. The NPY system in stress, anxiety and depression. Neuropeptides. 2004; 38(4):213–224. [PubMed: 15337373]
56. Heilig M, Koob GF. A key role for corticotropin-releasing factor in alcohol dependence. Trends Neurosci. 2007 Aug; 30(8):399–406. [PubMed: 17629579]
57. López AJ, Kramár E, Matheos DP, White AO, Kwapis J, Vogel-Ciernia A, et al. Promoter-Specific Effects of DREADD Modulation on Hippocampal Synaptic Plasticity and Memory Formation. J Neurosci. 2016 Mar 23; 36(12):3588–3599. [PubMed: 27013687]
58. Glangetas C, Girard D, Groc L, Marsicano G, Chaouloff F, Georges F. Stress switches cannabinoid type-1 (CB1) receptor-dependent plasticity from LTD to LTP in the bed nucleus of the stria terminalis. J Neurosci. 2013 Dec 11; 33(50):19657–19663. [PubMed: 24336729]
59. Sehlmeyer C, Schöning S, Zwitserlood P, Pfleiderer B, Kircher T, Arolt V, et al. Human fear conditioning and extinction in neuroimaging: A systematic review. PLoS One. 2009; 4(6)
60. Nagai M, Kishi K, Kato S. Insular cortex and neuropsychiatric disorders: a review of recent literature. Eur Psychiatry. 2007 Sep; 22(6):387–394. [PubMed: 17416488]
61. Shackman AJ, Fox AS. Contributions of the Central Extended Amygdala to Fear and Anxiety. J Neurosci. 2016; 36(31):8050–8063. [PubMed: 27488625]
62. Gungor NZ, Pare D. Functional Heterogeneity in the Bed Nucleus of the Stria Terminalis. J Neurosci. 2016; 36(31):8038–8049. [PubMed: 27488624]
63. Shackman AJ, Fox AS, Oler JA, Shelton SE, Davidson RJ, Kalin NH. Neural mechanisms underlying heterogeneity in the presentation of anxious temperament. Proc Natl Acad Sci. 2013; 110(15):6145–6150. [PubMed: 23538303]
64. Awwad HO, Gonzalez LP, Tompkins P, Lerner M, Brackett DJ, Awasthi V, et al. Blast Overpressure Waves Induce Transient Anxiety and Regional Changes in Cerebral Glucose Metabolism and Delayed Hyperarousal in Rats. Front Neurol. 2015; 6(June):132. [PubMed: 26136722]
65. Liu M-L, Liang F-R, Zeng F, Tang Y, Lan L, Song W-Z. Cortical-limbic regions modulate depression and anxiety factors in functional dyspepsia: a PET-CT study. Ann Nucl Med. 2012; 26(1):35–40. [PubMed: 21953211]
66. Pleil KE, Helms CM, Sobus JR, Daunais JB, Grant KA, Kash TL. Effects of chronic alcohol consumption on neuronal function in the non-human primate BNST. Addict Biol. 2015 Jul 29. n/a-n/a.
67. Marcinkiewcz, Ca, Dorrier, CE., Lopez, AJ., Kash, TL. Ethanol induced adaptations in 5-HT2c receptor signaling in the bed nucleus of the stria terminalis: implications for anxiety during ethanol withdrawal. Neuropharmacology. 2015; 89:157–167. [PubMed: 25229718]

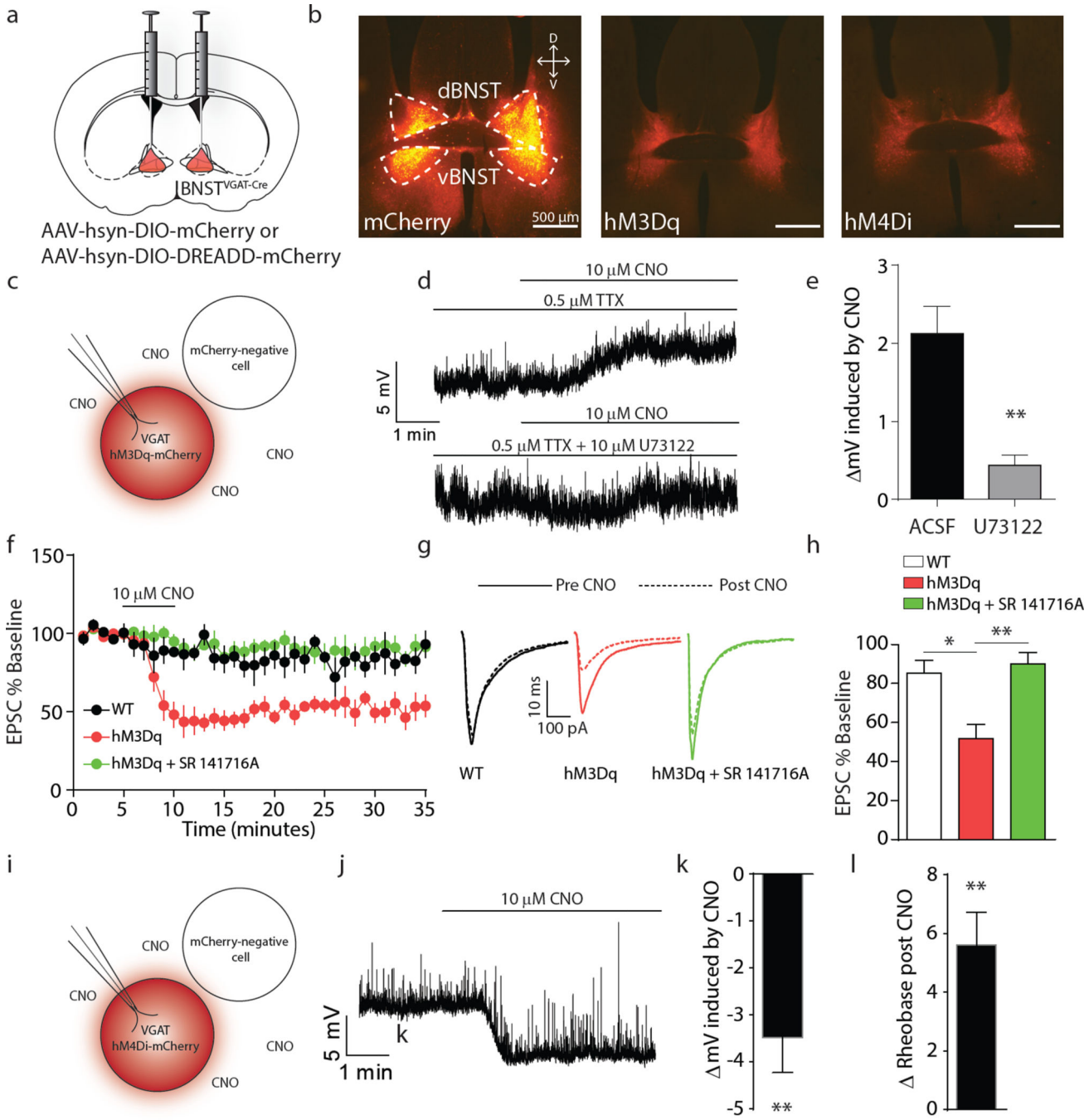

Figure 1.

Select modulation of BNST VGAT neurons using DREADDs. (**a**) Stereotaxic delivery of viruses encoding a Cre-inducible mCherry or DREADD (hM3Dq or hM4Di) into the BNST of VGAT-Cre mice. (**b**) Representative sections showing expression of a Cre-inducible mCherry (left), hM3Dq (middle), or hM4Di (right). Scale bars indicate 500 µm. (**c**) Schematic of *ex vivo* slice electrophysiology in hM3Dq-mCherry-expressing BNST neurons in the presence of CNO. (**d**) Representative traces from an hM3Dq-expressing BNST VGAT neuron depolarized by bath application of 10 µM CNO in the presence of TTX, but not in

the presence of the PLC inhibitor U73122. (**e**) Average change in resting membrane potential during the last 2 minutes of CNO application in ACSF + TTX with and without U73122 (right). *N*: ACSF, 6 cells from 4 mice; ACSF + U73122, 4 cells from two mice. (**f**) Time course of hM3Dq-induced reduction in evoked EPSCs is blocked by CB_1R antagonist SR 141716A. **, $p<0.01$, Mann Whitney test. Error bars indicate SEM. (**g**) Representative superimposed average evoked responses of the five minutes before CNO bath application (solid trace) and 20 to 25 minutes of washout (dotted line). (**h**) Mean evoked EPSC amplitude during minutes 30–35 (20–25 minutes of washout). $F_{(2,10)}=10.36$, $p=0.0037$. *$p<0.05$, Tukey's multiple comparison test; **$p<0.01$ Tukey's multiple comparison test. (**i**) Schematic of *ex vivo* slice electrophysiology in hM4Di-mCherry-expressing BNST neurons in the presence of CNO. (**j**) Representative tracing showing hyperpolarization of hM4Di-mCherry-expressing BNST neuron in the presence of 10 μM CNO. (**k**) Mean hyperpolarization induced by 10 μM CNO. **$p<0.01$, one-sample t-test. *N*: 10 cells from 6 mice. (**l**) Mean change in rheobase following bath CNO application. **$p<0.01$, one-sample t-test. *N*: 5 cells from 4 mice.

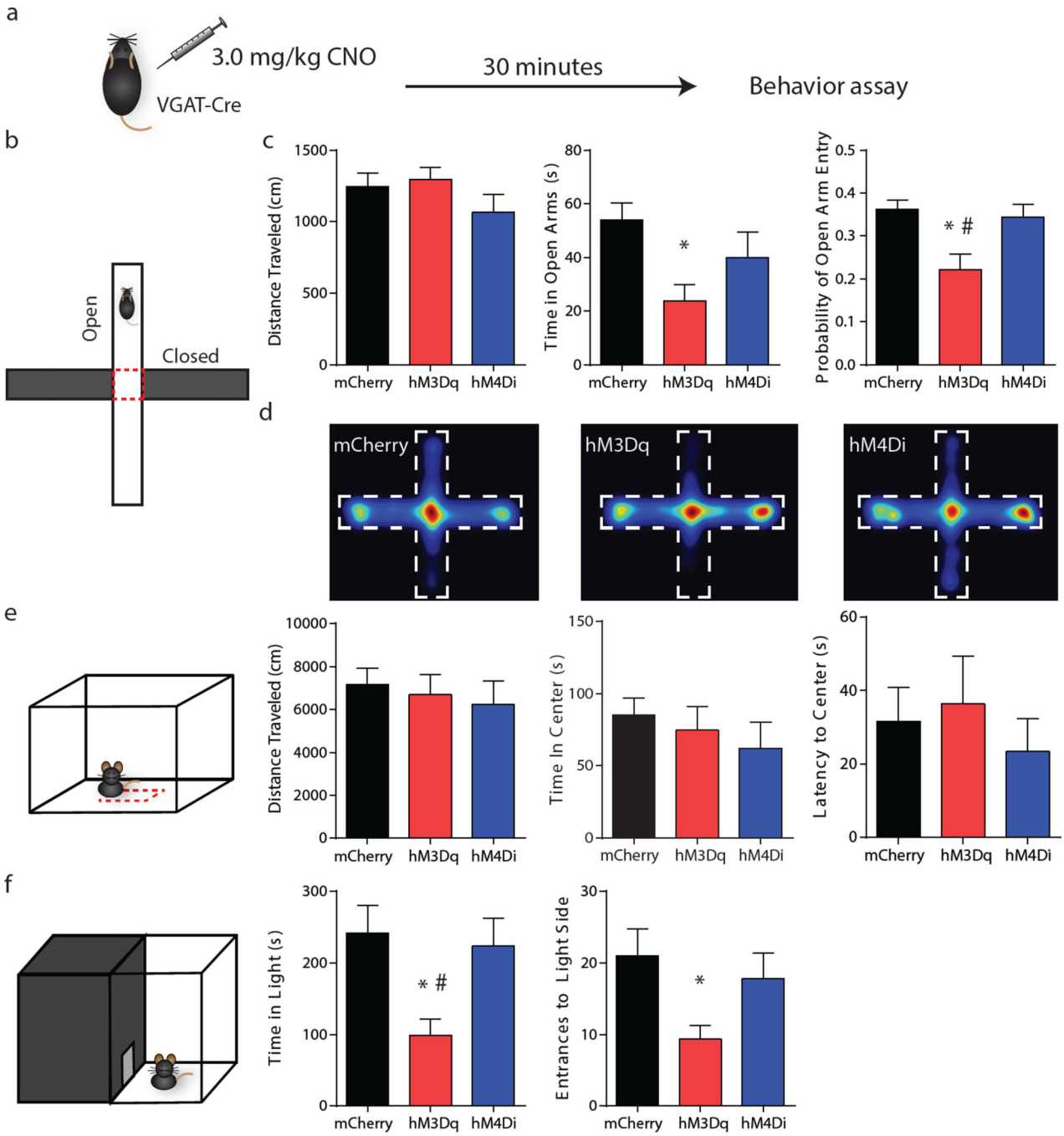

Figure 2.

Chemogenetic activation of BNST VGAT neurons increases anxiety-like behavior. (**a**) Behavioral assay design. VGAT-Cre mice expressing DIO-mCherry, DIO-hM3Dq, or DIO-hM4Di in the BNST were injected with 3.0 mg/kg CNO 30 minutes before being tested in exploratory assays. (**b**) Elevated plus maze (EPM). (**c**) Distance traveled (left; $F_{(2,23)}$=1.413, p=0.26), time in open arms (middle; $F_{(2,23)}$=3.894, p<0.05, One-Way ANOVA and Tukey's *post-hoc* test) and probability of an open arm entry (right; $F_{(2,23)}$=6.305, p<0.01, One-Way ANOVA, p<0.05, Tukey's *post-hoc* test) during a 5 minute EPM session. *N*: 8 mcherry, 9

hM3Dq, 9 hM4Di). (**d**) Averaged heat maps showing time spent in open and closed arms for mCherry (left), hM3Dq (center), and hM4Di (right) expressing mice. (**e**) Open field. Distance traveled (left; $F_{(2,18)}$=0.2503, p=0.78, One-Way ANOVA. *N*: 7 mCherry, 6 hM3Dq, 8 hM4Di), time in the center (middle; $F_{(2,18)}$=0.5538, p=0.58. *N*: 7 mCherry, 6 hM3Dq, 8 hM4Di), and latency to enter the center (right; $F_{(2,22)}$ = 0.3674, p=0.6967. *N*: 8 mCherry, 9 hM3Dq, 8 hM4Di) during a 30 minute open field session. (**f**) Light-dark box. Time in (left; $F_{(2,23)}$=5.266, p<0.05, One-Way ANOVA, p<0.05, Tukey's *post-hoc* test) and entrances to (right; $F_{(2,23)}$=3.629, p<0.05), One-Way ANOVA, p<0.05, Tukey's *post-hoc* test) the light compartment during a 15 minute session. *N*: 8 mCherry, 9 hM3Dq, 9 hM4Di. *p <0.05 relative to mCherry, # p<0.05 relative to hM4Di, Tukey's post hoc test. Error bars indicate SEM.

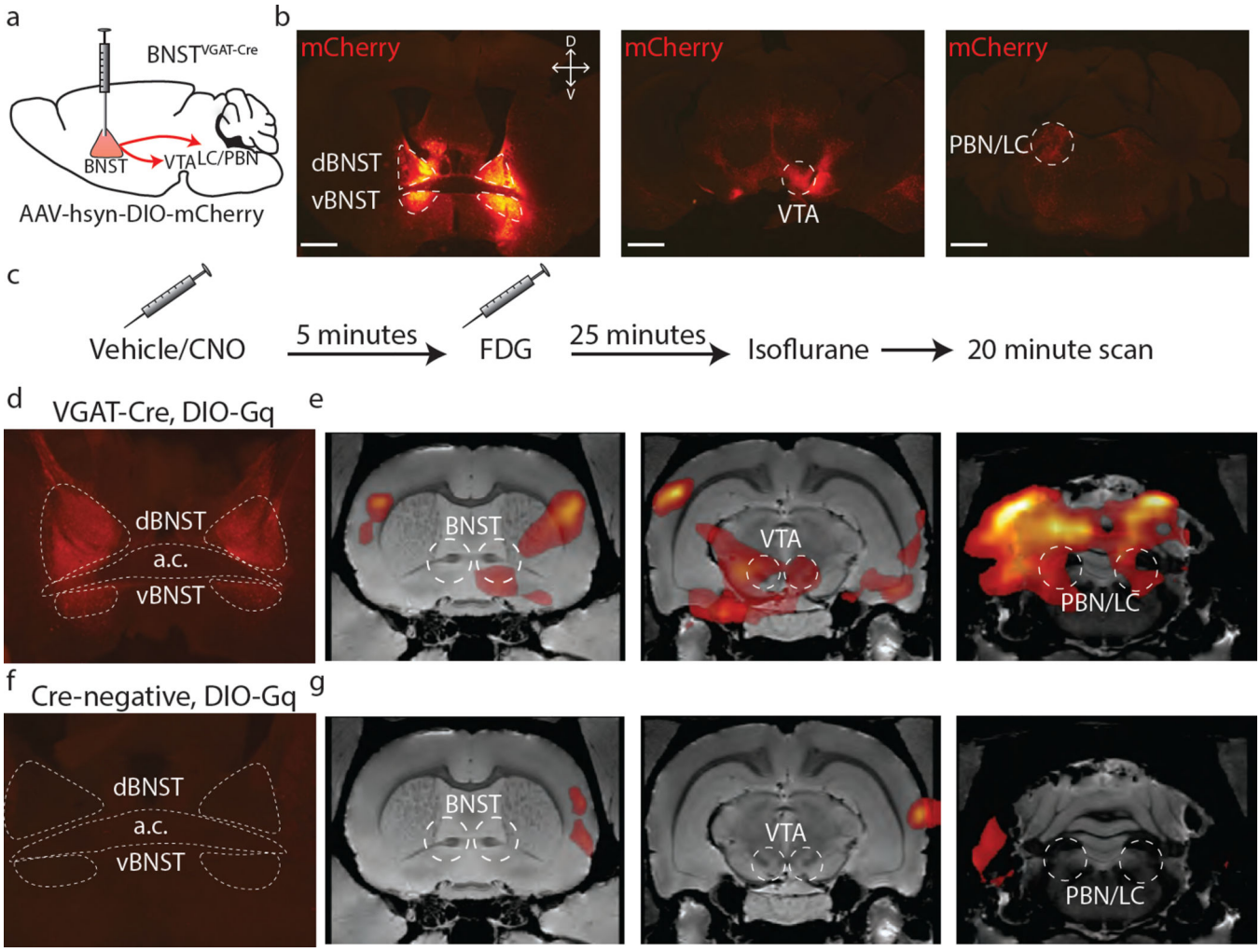

Figure 3.

Metabolic mapping of downstream activity following CNO-induced activation of hM3Dq in BNST VGAT neurons. (**a**) Injection of a DIO-mCherry to the BNST of a VGAT-Cre to label projection fibers. (**b**) mCherry fluorescence observed in the BNST injection site (left) and fluorescent fibers in the VTA (middle) and PB/LC (right). Scale bars: 1 mm. (c) μPET imaging timeline. Mice were injected with vehicle or CNO and five minutes later injected with FDG. 25 minutes later mice were anesthetized with isoflurane and placed on the scanning bed for a 20 minute scanning session. (**d**) Representative image of a DIO-hM3Dq-mCherry BNST injection site. Scale bar: 500 μm. (**e**) Increased FDG uptake in areas corresponding to the BNST (left) VTA (middle) and PB/LC (right) following activation of hM3Dq in BNST VGAT neurons. (**f**) Representative injection of a DIO-hM3Dq-mCherry to a Cre-negative control mouse. (**g**) No change in FDG uptake in the BNST (left), VTA (middle), or PB/LC (right) from pooled adjacent controls. *N*: 4 mice per group. A.c.: anterior commissure.

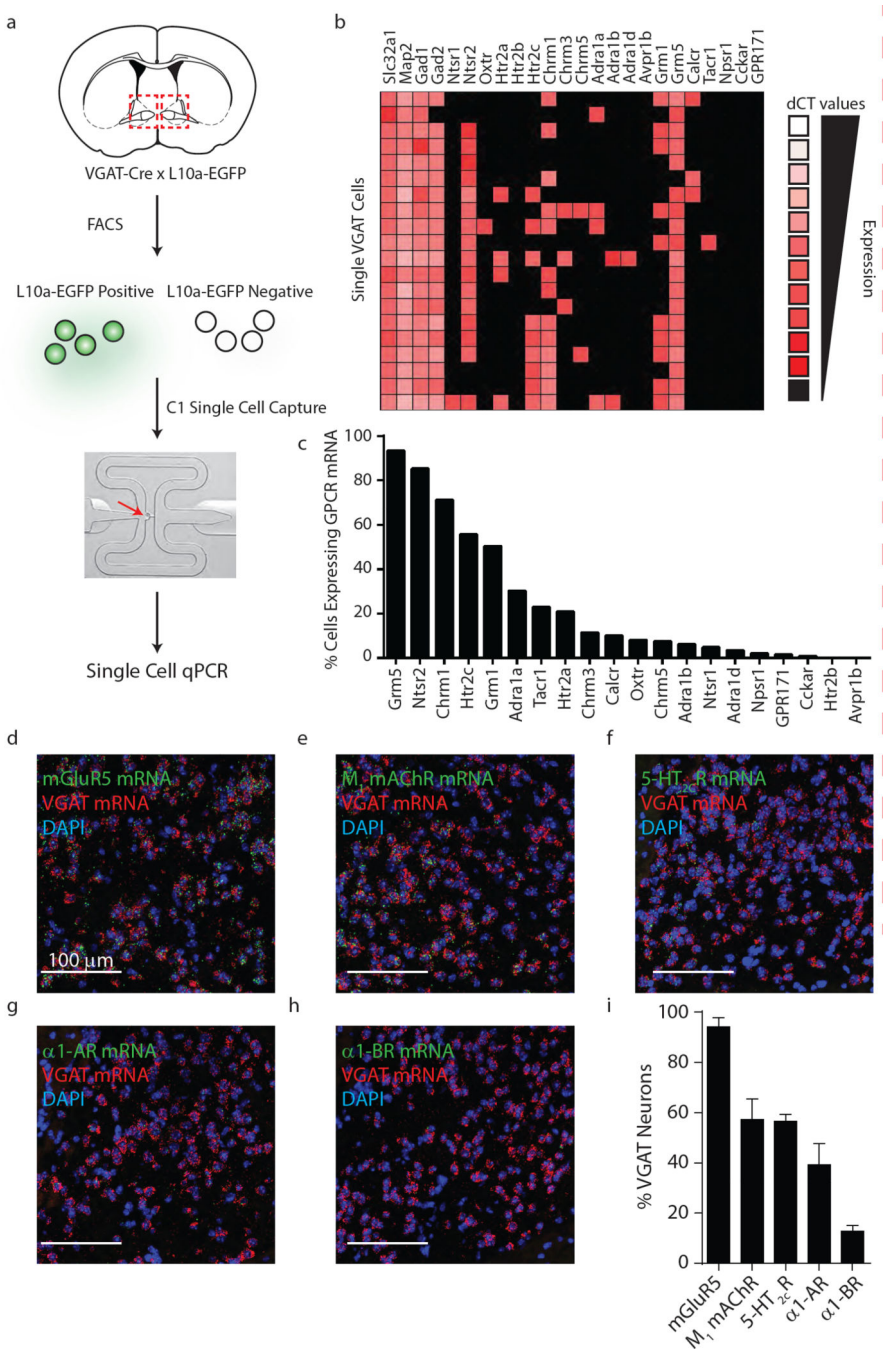

Figure 4.

Single-cell qPCR analysis reveals G_q-coupled GPCRs in BNST VGAT cells. (**a**) BNST tissue was dissected from a VGAT-Cre×L10-EGFP mouse and dissociated to create a single-cell suspension. Following FACS, individual EGFP-positive cells were captured on a C1 chip and used for single-cell qPCR with probes targeting G_q-coupled receptors. (**b**) Heat map depicting delta Ct values of individual probes from 149 cells positive for Slc32a1, Map2, and Gad1 and/or Gad2. Values are normalized to RN18S. (**c**) Percent of cells expressing transcripts for each G_q-coupled GPCR. (**d–h**) Representative fluorescent *in situ*

hybridization sections for assessing colocalization of VGAT mRNA and mRNA for mGluR5 (d), M_1mAchR (e), 5-HT_{2C}R (f), α1-AR (g), α1-BR (h). Scale bar: 100 μm. (**i**) Percent of VGAT mRNA positive cells expressing various GPCR transcripts. Error bars indicate SEM. *Gene* (Protein): *Grm5* (MGLUR5), *Ntsr2* (NTSR2), *Chrm1* (CHRM1), *Htr2c* (HTR2C), *Grm1* (mGluR1), *Adra1a* (α1-AR), *Tacr1* (TACR1), *Htr2a* (5-HT_{2A}R), *Chrm3* (M_3 mAChR), *Calcr* (CT), *Oxtr* (OXTR), *Chrm5* (M_5 mAChR), *Adra1b* (α1-BR), *Ntsr1* (NTSR1), *Adra1d* (α1-DR), *Npsr1* (NPSR1), *Gpr171*(GPR171), *Cckar* (CCKAR), *Htr2b* (5-HT_{2B}R), *Avpr1b* (AVPR1B).

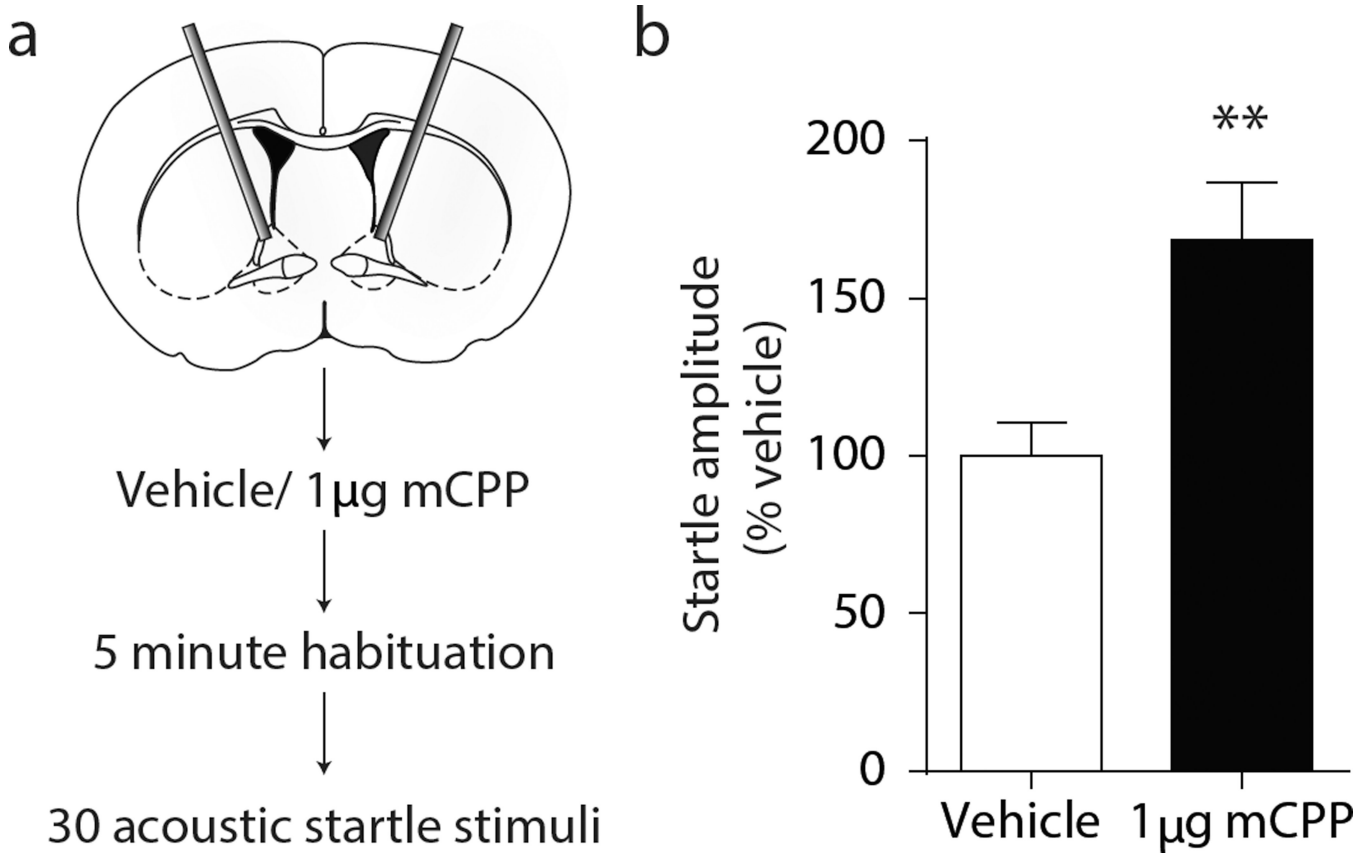

Figure 5.

Local infusion of mCPP to the BNST increases acoustic startle. (**a**) Mice with cannulae inserted over the BNST received an infusion of 1 µg mCPP and were immediately placed in the acoustic startle chamber. Following a 5 minute habituation period, mice were presented with 30 startle stimuli. (**b**) Mice treated with mCPP showed an exacerbated acoustic startle response ($t(14) = 3.015$, $p = 0.0093$). *N*: 7 vehicle, 9 mCPP. $^{**}p<0.01$, unpaired t-test. Error bars indicate SEM.